Coimbra Solar Physics Meeting on The Physics of Chromospheric Plasmas
ASP Conference Series, Vol. xxx, 2007
Petr Heinzel, Ivan Dorotovič and Robert J. Rutten, eds.

Semiempirical Models of Solar and Stellar Active Chromospheres

Pablo Mauas

Instituto de Astronomía y Física del Espacio, Buenos Aires, Argentina

Abstract. Semiempirical models have been used for decades to study the chromospheres of the Sun and of stars of different spectral types. These models are built to match the observations in different spectral features, and make no assumption about the physical processes responsible for the heating of the chromosphere, but can be used to constrain these processes.

In this paper we review some of the work done in the modeling of solar and stellar atmospheres, in particular to study active phenomena: solar and stellar flares and chromospheres of stars of different activity levels. We also review an application to RGB stars, where this technique allowed the detection of a stellar wind.

1. Introduction

Semiempirical models have been used for decades to study the solar chromosphere, and those of stars of different spectral types. These models describe the variations of the essential parameters across the chromosphere, starting from a distribution of T vs. height (or column mass), built to explain the observations in several spectral features (continua or line profiles). To build a semiempirical model, there is no assumption *a priori* about the physical process responsible for the heating of the chromosphere, but the results of the models can be used to constrain these processes.

To build the model, it is usually assumed a homogeneous atmosphere, in static or quasi static equilibrium. Regarding the homogeneity, it refers to different scales when different features are modeled. In the solar case, the scale is usually fixed by the resolution of the observations under study, and it is different for models of the mean solar chromosphere, of active regions, or for particular flare kernels. In the stellar case, on the other hand, observations do not allow to separate different stellar structures, and therefore it is usually assumed a homogeneous chromosphere covering all the star. However, in a few cases two components were assumed. For example, when studying a flare on the dMe star Ad Leo, Mauas & Falchi (1996) modeled the flaring kernel assuming different filling factors, and used the atmosphere for the quiet star obtained to match observations taken during the quiescent state (Mauas & Falchi 1994).

Therefore, these models give information on a "mean" state of the atmosphere, both temporal and spatially. For example, Fontenla et al. (2006) built "semiempirical models of the solar photosphere at spatial resolution of a few arcseconds and temporally averaged over several p-mode oscillation periods". It is important to keep in mind that the "mean" structure obtained is

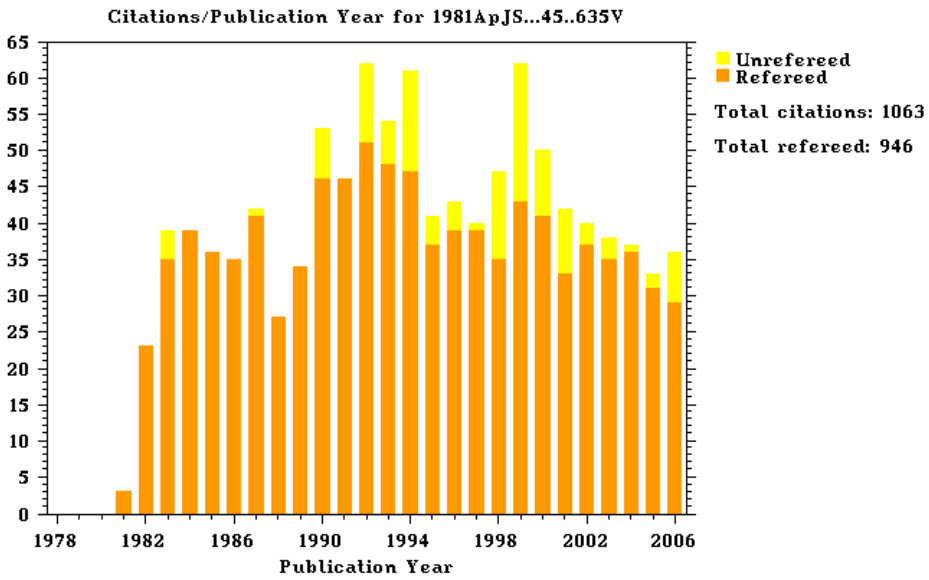

Figure 1. Citation history of the paper by Vernazza et al. (1981), obtained from the ADS in December 2006.

weighted by the effect on the emitted radiation, in particular on the features under study.

The most important problem of this approach lies in the uniqueness of the models computed in this way. In fact, knowing that a particular atmosphere would emit a line profile like the one we observe for a given star does not imply that the star has indeed this atmospheric structure, since we do not know whether some other atmosphere would produce the same profile. To solve, or at least to reduce, this problem, the modeling has to be based in several spectral features, with different regions of formation. Usually, Ca II K and Hα (or another Balmer line) are used. However, in this case the higher part of the chromosphere is left undefined, except in very active situations (for a thorough discussion of this problem, see Mauas 2000).

2. Solar models

Certainly the best known semiempirical model is the one for the average Quiet-Sun, Model C by Vernazza et al. (1981). In fact, this is one of the most cited papers of Solar Physics, as can be seen in Fig. 1, which shows its citation history obtained from the ADS.

In that work, the authors used EUV Skylab observations to determine separate chromospheric models for six brightness components, ranging from a dark cell center to a very bright network element. These models were built to match Ly-α, Ly-β, the Lyman continuum, and other continua.

Later on, this model was modified, in particular in the temperature minimum region, by Maltby et al. (1986), who computed semiempirical models for

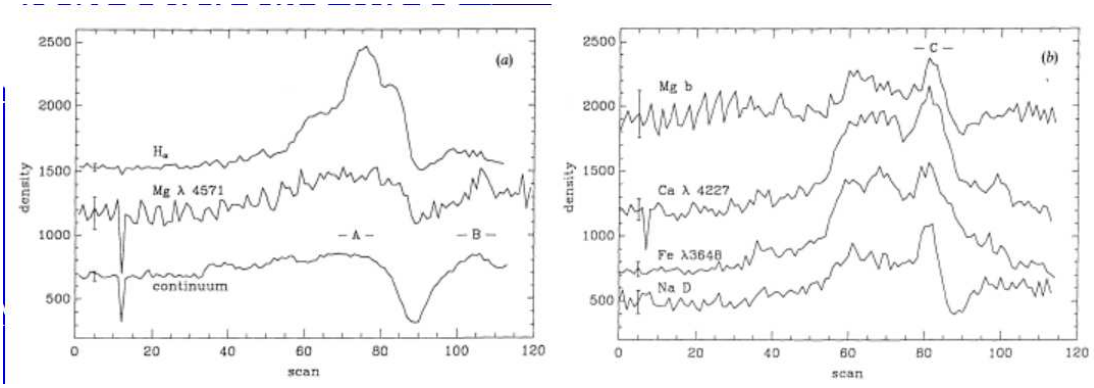

Figure 2. Microdensitometer scans made in the direction across the dispersion, for a continuum window and several spectral lines (Mauas et al. 1990).

sunspot umbrae. More recently, this model has been updated in a series of papers by Fontenla et al. (1990, 1991, 1993, 2002).

Fontenla et al. (1999) built models for different solar features, including sunspots, plage, network, and the quiet atmosphere. This kind of work provides an understanding of the sources of variability arising from solar-activity surface structures. In fact, the output of these models was used to study variations of the solar irradiance, a subject of particular interest for solar-terrestrial studies.

More details about ongoing work in the modeling of different features of the solar atmosphere can be found in the presentations by Avrett and Fontenla in these proceedings.

3. Solar flare models

The first semiempirical models of solar flares were constructed by Machado & Linsky (1975), to approximately simulate observations of flares. They studied in particular the Ca II lines, using their wings to derive models of the upper photosphere of the flare. Later, Lites & Cook (1979) built a semiempirical model of the chromosphere between 5500 and 100,000 K during a flare, based on its ultraviolet spectra.

Perhaps the best known semiempirical flare models are the ones by Machado et al. (1980), who built two models representative of bright and fainter flares, and not for specific events. Their models reproduced observations in lines and continua of H I, Si I, C I, Ca II, and Mg II. They found that the minimum temperature is located deeper and is higher than in the quiet-sun and active-region models. They concluded that substantial Ly-α radiative back-heating occurs in the upper chromosphere resulting from the conductive energy flux in the transition zone where the Ly-α line cools the gas.

Gan & Fang (1987) started a series of semiempirical models to study the influence of the chromospheric condensation in the energy balance of the flaring atmosphere (see also Gan et al. 1993). In particular, Gan & Mauas (1994) found that the back-warming of the atmosphere is enhanced by the condensation, and may be very effective to heat the region of the temperature minimum and the

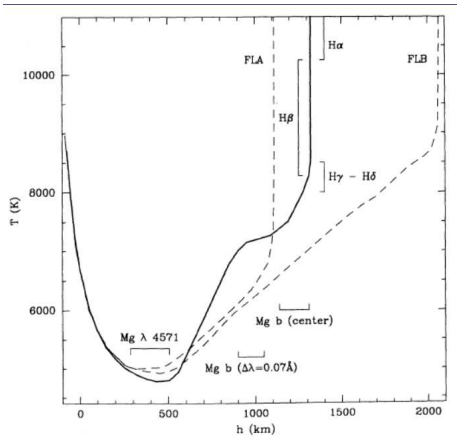

Figure 3. Models for the three kernels, and height of formation of different lines (Mauas et al. 1990)

upper photosphere, as deep as h = 0 km, resulting in an enhancement of the continuum emission.

Later, Mauas et al. (1990) and Mauas (1990, 1993) studied different regions of a white light flare, and built the first semiempirical models of a WLF which are consistent not only with observations of the continuum emission level but also with a set of spectral lines having heights of formation which span the chromosphere and upper photosphere. The regions studied can be seen in Fig. 2, which shows microdensitometer scans made in the direction across the dispersion, in spectral features formed at different heights in the atmosphere.

In the figure, three distinct kernels can be seen: Kernel A is the brightest in Hα, and one of the brightest in the continuum. Kernel B, on the other hand, is bright in white light but not in Hα. Finally, kernel C is the brightest in the lines which are formed in the mid-chromosphere, but it is not the brightest in Hα, and is even darker in the continuum.

In Fig. 3 the models for the three kernels are shown. Finally, Fig. 4 shows a comparison, for one kernel, of the computed emission for the continuum and the two first Balmer lines with the observations.

Regarding the two white-light kernels, A and B, the models are not compatible with the hypothesis that the continuum emission is caused by enhanced Balmer and Paschen hydrogen continua, and they present strong evidence instead that the emission is of photospheric origin and that its source is due to H^-. The observation and the models derived from them showed that white-light emission can occur in areas of the active region where there is no chromospheric emission and in particular no Hα emission. This fact seems to rule out the viability of downward transport mechanisms as the source of the energy required for the WLF.

One of the results that can be derived from this kind of models, is the cooling rate Φ, which is the net energy radiated by the main spectral features. This cooling rate can be used to constrain the energy needed to heat the atmosphere. In Fig. 5 a detail of Φ for the model for the mid-chromospheric kernel, is compared to the energy deposited by different electron beams (which was computed

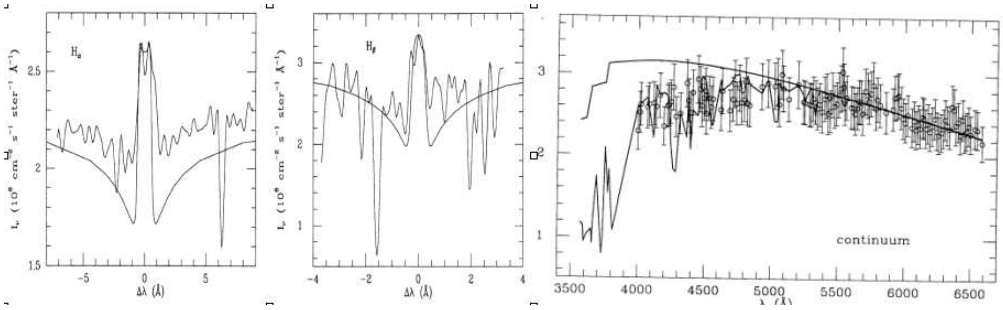

Figure 4. Computed emission in Hα, Hβ and the continuum for Kernel A. In the continuum window, the lower and upper curves show the emission computed with and without line-blanketing, respectively (Mauas et al. 1990).

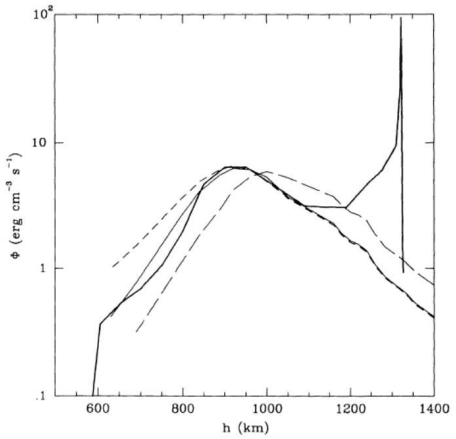

Figure 5. The cooling rate for the mid-chromospheric kernel, compared with the energy deposited by different electron beams (Mauas 1993).

using the method developed by Gomez & Mauas 1992; Mauas & Gomez 1997). It can be seen that the match is very good for a particular beam, and therefore that this method can be used to effectively constrain the heating mechanism in this region.

Another application of this kind of modeling is to include velocity fields, trying to reproduce the observed line asymmetries, and in this way to further constrain the processes that take place during flares. To do so, Falchi & Mauas (2002) studied the chromospheric structure of a small flare, before, during and after the fist hard X-ray spike. They constructed 5 semiempirical models for different times, to reproduce the profiles of the Hα, Ca II K and Si I 3905 lines during the flare evolution. The lines were chosen because their heights of formations span the whole atmosphere, to avoid indetermination in the deduced chromospheric structure and in the velocity field.

In Fig. 6 a comparison between observed and computed profiles can be seen, and shown in Fig. 7 are the evolution in time of the temperature T, of the electron density $n_{\rm e}$, and of the velocity v at two points in the atmosphere, one at ≈ 900 and another at ≈ 1400 km. Also shown is the evolution of the coronal

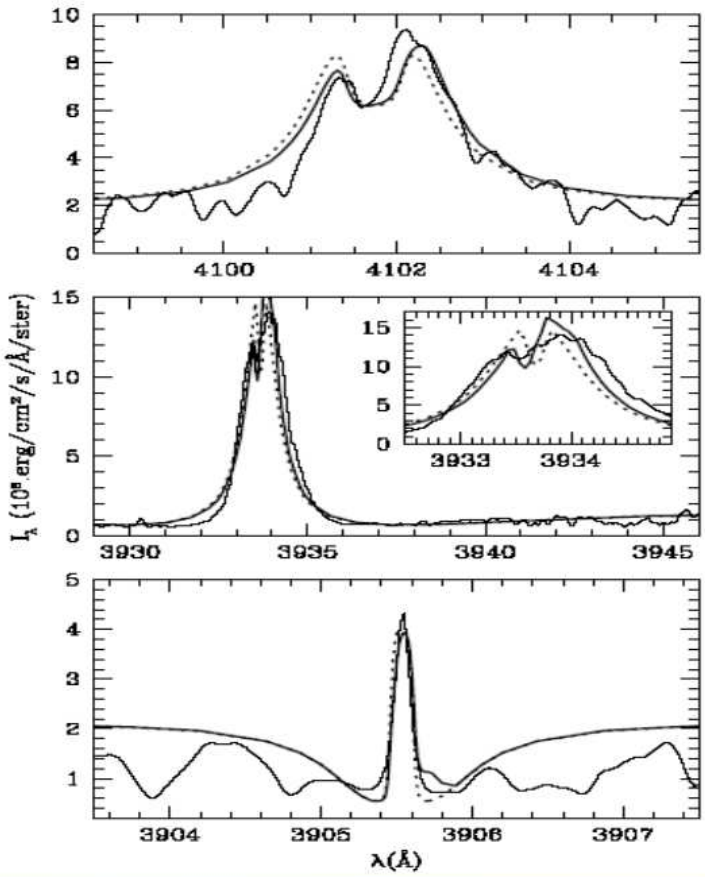

Figure 6. An example of the match obtained between computed and observed profiles, with a velocity field to reproduce the line asymmetries. Upper panel: Hα. Mid panel: Ca II K. Lower panel: Si I (Falchi & Mauas 2002).

pressure $P_{\rm cor}$. It can be seen that that the whole chromosphere undergoes a strong upward motion within 1 s of the maximum of the first hard X-ray spike, when the temperature and the density begin to rapidly increase. This seems the first chromospheric response to the energy deposition and/or release. Only 6 s after the hard X-ray peak, a strong downflow begins in the low chromosphere and its velocity continues to increase even during the cooling phase.

Another study of the evolution of chromospheric velocity fields during solar flares was done by Berlicki et al. (2005), who built a grid of models and fitted the observed profiles of the Hα line (see also the paper by Berlicki in these proceedings).

4. Models for solar analogues

The same technique was successfully applied to the modeling of the atmospheres of cool stars. In particular, there has been extensive modeling of dM stars, start-

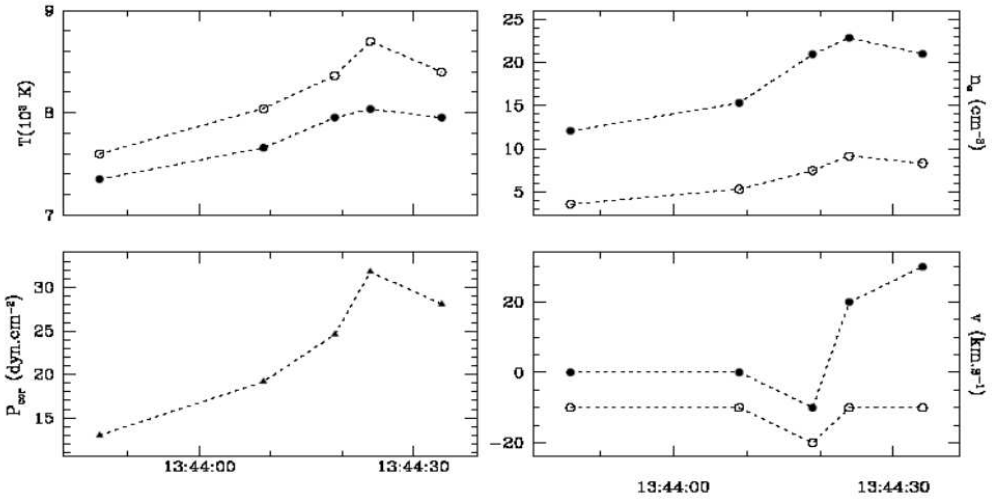

Figure 7. Evolution of temperature, electron density and velocity in two points of the atmosphere, one in the mid-chromosphere (full dots), and another at the base of the transition region (empty dots). Also shown is the evolution of the coronal pressure (Falchi & Mauas 2002).

ing perhaps with the work by Cram & Mullan (1979). In particular, modeling of the quiescent state of dM stars was done by the Armagh group (see Short & Doyle 1998, and references therein), and by Mauas & Falchi (1994), and Mauas et al. (1997). Also, flares in these stars were studied by the same groups (Mauas & Falchi 1996; García-Alvarez et al. 2002).

More recently, Vieytes et al. (2005) built models for the Sun as a star and 9 stars with the same color than the Sun and, therefore, the same photosphere, and different levels of activity, which implies different chromospheric structures. The models were built to match the Hβ, Ca II K, Na D and Mg b line profiles, and a velocity field was added when needed to match the asymmetry in the K line.

In Fig. 8 the resulting models are shown, and in Fig. 9 the profiles for two stars, a very inactive and a very active one, are compared to the observations. Note that in the second case, an asymmetry in the K line is observed, and a velocity field was included to match it.

This model was later complemented with a similar one, where K stars of different activity levels were constructed (Vieytes et al, A&A *submitted*. The main result of both papers is shown in Fig. 10, where the cooling rate Φ, computed from the models, integrated over all the chromosphere, and normalized by the bolometric luminosity $L = \sigma.T_{eff}^4$, is plotted against S in Fig. 10. S is the most usual index of stellar chromospheric activity, which is essentially the flux in the Ca II H+K lines normalized by the continuum nearby. From the figure, it can be seen that this index is, indeed, a good proxy for activity, since it is a good indicator for the ratio between the energy radiated in the chromosphere and the total luminosity.

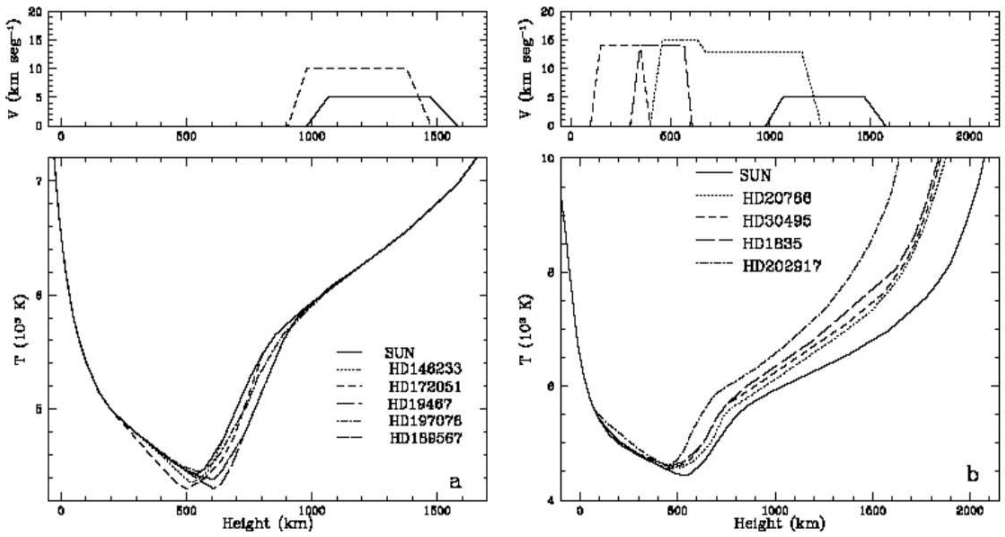

Figure 8. Models of the least active stars (left) and for the most active stars. Top: macroscopic velocity fields for the corresponding star (Vieytes et al. 2005).

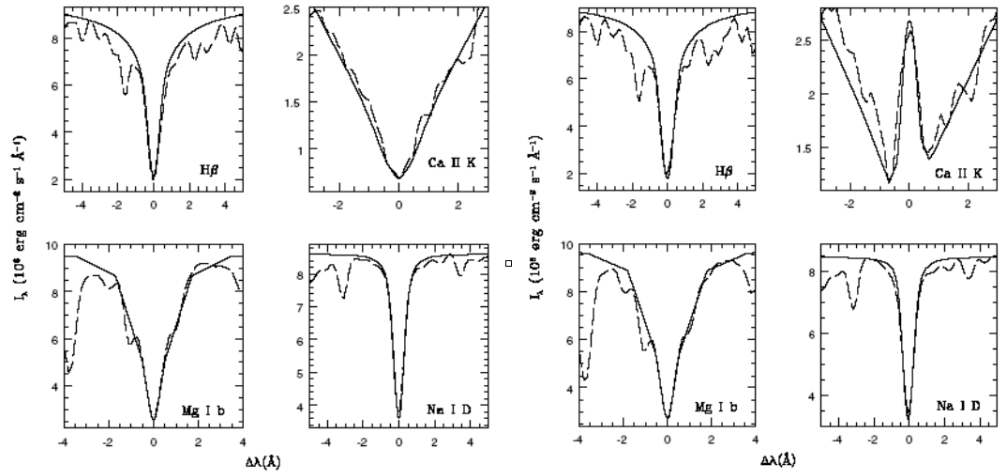

Figure 9. Observed (dashed line) and synthetic (full line) profiles for two stars. Left: HD19467. Right: HD 1835.

This S index is the one defined in the largest observational study of stellar chromospheric activity, which is the one started in 1966 at the Mount Wilson Observatory using a four channel spectrometer to measure the emission in the core of the H and K lines of Ca II and in two continuum windows nearby. Emission in these lines, by analogy with the Sun, is assumed to be well correlated with surface magnetic fields and, therefore, with activity.

Qualitative studies of this data by Vaughan & Preston (1980) suggested that a "gap" in chromospheric emission exists for stars in the range $0.45 \leq$

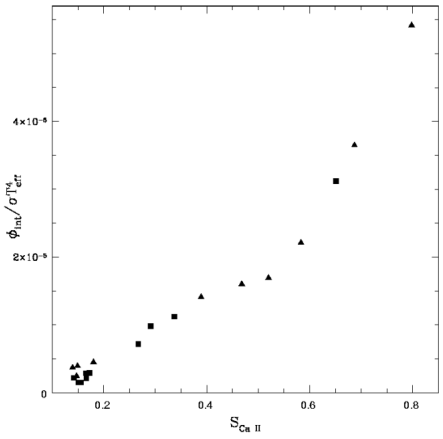

Figure 10. $\Phi_{int}/\sigma.T_{eff}^4$ vs S for K and G stars

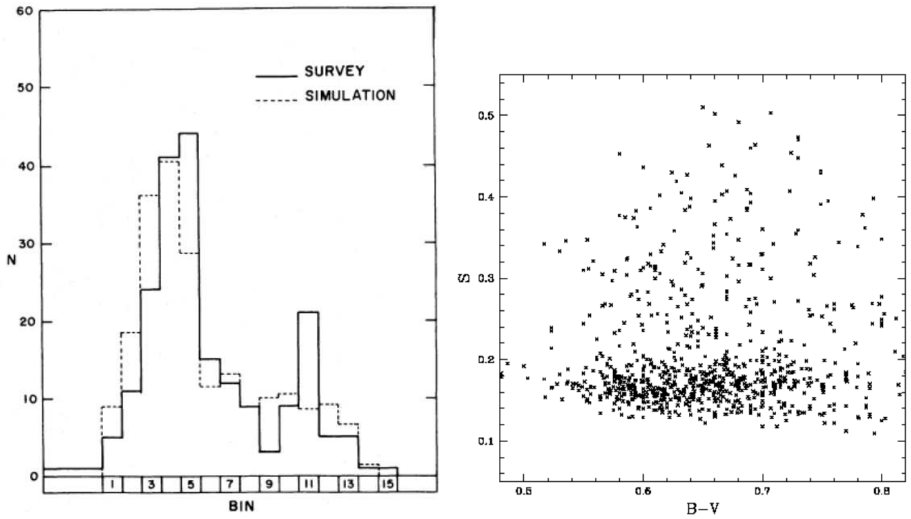

Figure 11. Left panel: Distribution of stars with different levels of activity. A gap for $0.2 \leq S \leq 0.3$ is evident (Vaughan & Preston 1980). Right panel: The results of the survey by Henry et al. (1996), for southern stars.

$B-V \leq 1.0$. There are relatively large numbers of stars in this color range with either strong or weak chromospheric emission, but relatively few with moderate emission. Their results can be seen in the left panel of Fig. 11.

In a survey of Ca II emission in southern solar-type stars, Henry et al. (1996) also found a bimodal distribution, although they considered it "more of a transition zone than a gap", and that "there is not a complete absence of stars" in it. In fact, the right panel of Fig. 11 shows their results. It can be seen that there is a large number of stars with $0.1 < S < 0.2$, and a lower number of stars with $S > 0.2$.

Much has been speculated on the origin of this gap, usually called the Vaughan-Preston (VP) gap in the literature. For example, since chromospheric

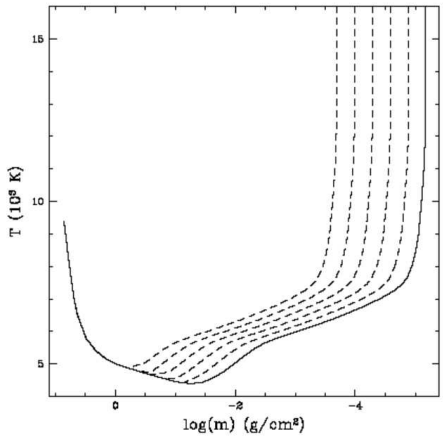

Figure 12. Some of the atmospheric models. The full line is the quiet Sun model C by Fontenla et al. (1993) and the dashed lines are the models built by shifting this model by $\Delta \log(m)$= 0.3, 0.6, 0.9, 1.2 and 1.5 (Vieytes & Mauas 2004).

activity decreases with increasing stellar age, the VP gap could represent a change in the nature of activity at a certain stellar age (Knobloch et al. 1981, Soderblom 1982). Similarly, Hartmann et al (1984) interpreted the break in chromospheric activity as a fluctuation in the local stellar birthrate.

Alternatively, since activity is closely related to stellar rotation through the stellar dynamo generating the surface magnetic fields, Durney et al (1981) suggested that the VP gap can be due either to a rapid spindown at some point of stellar evolution, or to an abrupt change of the efficiency of the dynamo for a given rotation period. Other interpretations in terms of dynamo theory can be found in Soon et al. (1993) and Baliunas et al. (1996). Brandenburg et al (1998) also proposed a break in the rotation period around age 2-3 Gyr, roughly at the VP gap. Rocha-Pinto and Maciel (1998) suggested that the VP gap is related to an abrupt change in the metallicity distribution of these stars.

To investigate the response of the Ca II lines to the changes in the chromospheric structure induced by stellar activity, Vieytes & Mauas (2004) built a set of chromospheric models for stars with the same photospheric structure than the Sun and different activity levels. To do so, active stellar chromospheres were generated starting from the solar model C (Fontenla et al. 1993), and shifting inwards by a fixed $\Delta \log(m)$the T vs. log(m) structure in the chromosphere, down to the height below T_{min} where the original temperature is higher. Some of these models are shown in Fig. 12.

From the computed models, the values of S were obtained integrating the Ca II profiles, These S values are shown in Fig. 13 as a function of $\Delta \log(m)$. It can be seen that the activity index has a bimodal behavior, changing slope at about $\Delta \log(m)$=0.7, where $S \approx 0.2$.

This change in behavior can explain why there is a much larger number of stars with $S < 0.2$, since all stars having $\Delta \log(m)$<0.7 are in this region, and stars already having $\Delta \log(m)$>0.8 are already well above this value. To further check this assumption, the distribution of the values of S was computed, under

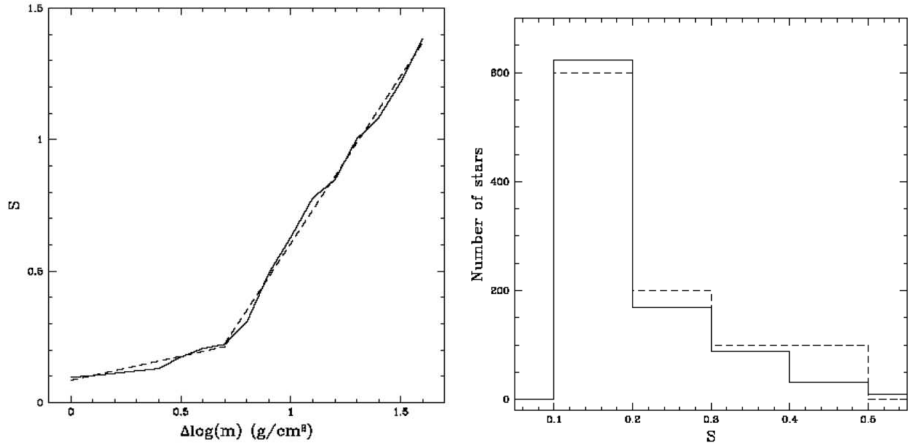

Figure 13. Left: The response of the Ca II S index to the different atmospheric models of Fig. 12. Also shown as dashed lines are the linear fits to the two different regimes (see text). Right: The full line is the histogram of S values for the survey by Henry et al. (1996) and the dashed line is the histogram of the computations by Vieytes & Mauas (2004), conveniently scaled.

the assumption that all models have the same possibility to occur in nature. In the right panel of Fig. 13 this distribution is compared with the distribution of the sample by Henry et al. (1996) shown in the right panel of Fig. 11, which has more than 900 observations. It can be seen that the agreement between both distributions is remarkable.

5. Chromospheres and mass loss in red giant stars

Stellar evolution theory requires some mass loss by Population II stars during the evolutionary phases preceding the horizontal branch (HB) phase, in order to account for (1) the observed morphologies of the HB in globular clusters, and the maximum luminosity reached by stars on the asymptotic giant branch. However, direct evidence for mass loss in these stars has been quite elusive.

In these stars, usually the profiles of the main chromospheric lines (Ca II and Hα) are asymmetric, which is an evidence of mass motions. Mauas et al. (2006) modeled 5 stars with clear evidence of emission in the Hα wings and at the bottom of the Ca II K absorption core (K_2 reversal). To reproduce the observed asymmetries, the models include the appropriate velocity fields.

Since the observed profiles for the stars were very similar, and differed mainly in the amount of asymmetry in the K_2 and Hα emission wings, it was possible to fit all the profiles with only two T vs. log(m) distributions, and different velocity fields. The computed profiles for one of the stars are compared with the observations in Fig. 14. Also shown are the profiles computed for the corresponding model without including the velocity field, as a reference for clarity.

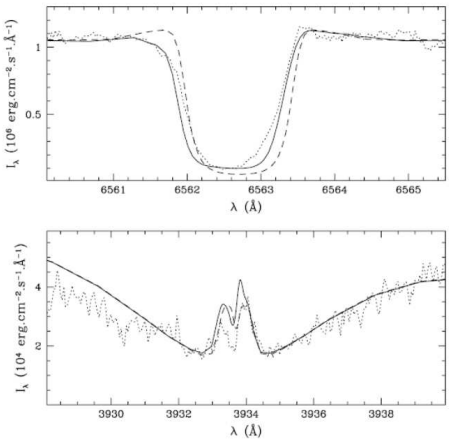

Figure 14. Observed (dotted) and computed (full) profiles for one of the RGB stars. Also shown for reference is the profiles computed without any velocity field.

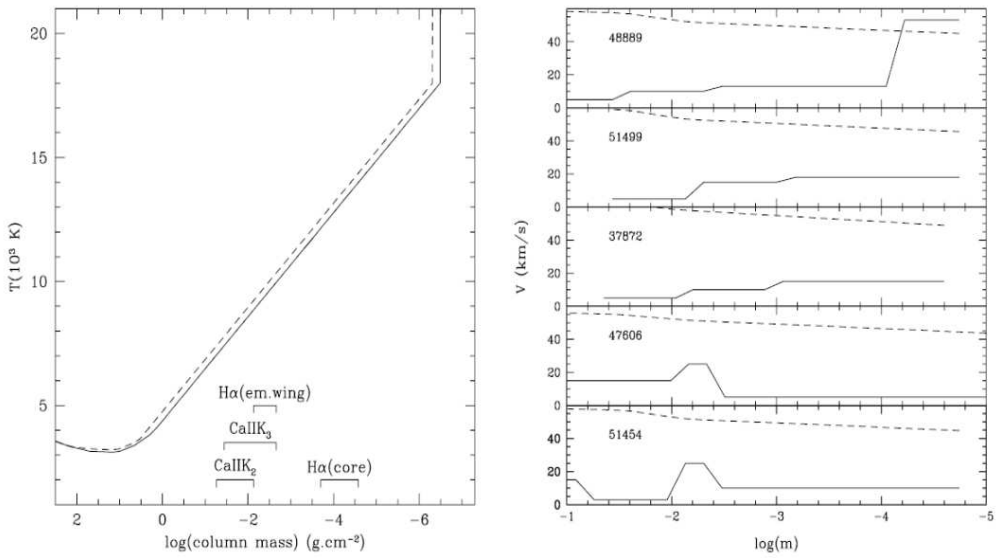

Figure 15. Left: The chromospheric models for the RGB stars. The approximate depth of formation of the Hα core and wings, and of the Ca II K_2 and K_3 line components are also indicated. Right: The velocity as a function of depth (solid line), derived from the best match with the Ca K and Hα lines, compared to the corresponding escape velocity (dashed line) (Mauas et al. 2006).

The models and the velocity fields are shown in Fig. 15. For comparison, the corresponding escape velocity is also shown. It can be seen that for one of the stars (star 48889) the expansion velocity at the most external point that can be modeled is larger than the escape velocity. This implies that, at least for this star, the material above this level is escaping from the atmosphere.

For the other stars, the expansion velocity estimated for the outermost modeled point, is smaller than the escape velocity at that depth. However, there is a mass outflow at this height, and the velocity is increasing in all cases, while, of course, the escape velocity is decreasing. Furthermore, there are no signs of a reversal in the velocity field, *i.e.* there is no material falling back in. Therefore, the most probable situation is that the velocity continues to increase, until eventually it reaches the escape velocity.

Therefore, these models confirm the existence of the stellar wind required by the theory. Furthermore, from the estimated velocity, and the column mass at the outermost point, the mass-loss rate can be estimated. It turns out that these rates are in agreement with the ones expected from stellar evolution theory.

Acknowledgments. I would like to thank Marcos Machado, Gene Avrett, and Ambretta Falchi. Without them, this work would not have been possible.

References

Berlicki A., Heinzel P., Schmieder B., Mein P., Mein N., 2005, A&A 430, 679
Cram L. E., Mullan D. J., 1979, ApJ 234, 579
Falchi A., Mauas P. J. D., 2002, A&A 387, 678
Fontenla J., White O. R., Fox P. A., Avrett E. H., Kurucz R. L., 1999, ApJ 518, 480
Fontenla J. M., Avrett E., Thuillier G., Harder J., 2006, ApJ 639, 441
Fontenla J. M., Avrett E. H., Loeser R., 1990, ApJ 355, 700
Fontenla J. M., Avrett E. H., Loeser R., 1991, ApJ 377, 712
Fontenla J. M., Avrett E. H., Loeser R., 1993, ApJ 406, 319
Fontenla J. M., Avrett E. H., Loeser R., 2002, ApJ 572, 636
Gan W. Q., Fang C., 1987, Solar Phys. 107, 311
Gan W. Q., Mauas P. J. D., 1994, ApJ 430, 891
Gan W. Q., Rieger E., Fang C., 1993, ApJ 416, 886
García-Alvarez D., Jevremović D., Doyle J. G., Butler C. J., 2002, A&A 383, 548
Gomez D. O., Mauas P. J., 1992, ApJ 398, 682
Henry T. J., Soderblom D. R., Donahue R. A., Baliunas S. L., 1996, AJ 111, 439
Lites B. W., Cook J. W., 1979, ApJ 228, 598
Machado M. E., Avrett E. H., Vernazza J. E., Noyes R. W., 1980, ApJ 242, 336
Machado M. E., Linsky J. L., 1975, Solar Phys. 42, 395
Maltby P., Avrett E. H., Carlsson M., Kjeldseth-Moe O., Kurucz R. L., Loeser R., 1986, ApJ 306, 284
Mauas P. J. D., 1990, ApJS 74, 609
Mauas P. J. D., 1993, ApJ 414, 928
Mauas P. J. D., 2000, ApJ 539, 858
Mauas P. J. D., Cacciari C., Pasquini L., 2006, A&A 454, 609
Mauas P. J. D., Falchi A., 1994, A&A 281, 129
Mauas P. J. D., Falchi A., 1996, A&A 310, 245
Mauas P. J. D., Falchi A., Pasquini L., Pallavicini R., 1997, A&A 326, 249
Mauas P. J. D., Gomez D. O., 1997, ApJ 483, 496
Mauas P. J. D., Machado M. E., Avrett E. H., 1990, ApJ 360, 715
Short C. I., Doyle J. G., 1998, A&A 336, 613
Vaughan A. H., Preston G. W., 1980, PASP 92, 385
Vernazza J. E., Avrett E. H., Loeser R., 1981, ApJS 45, 635
Vieytes M., Mauas P., Cincunegui C., 2005, A&A 441, 701
Vieytes M., Mauas P. J. D., 2004, Ap&SS 290, 311